Experimental validation of a Monte Carlo proton therapy nozzle model incorporating

magnetically steered protons

Experimental validation of a Monte Carlo proton therapy nozzle model incorporating magnetically steered protons

S W Peterson[1,3]**, J Polf**[1]**, M Bues**[2]**, G Ciangaru**[2]**, L Archambault**[1]**, S Beddar**[1] **and A Smith**[2]

[1] Department of Radiation Physics, Unit 94, The University of Texas M D Anderson Cancer Center, 1515 Holcombe Blvd., Houston, TX 77030, USA
[2] Proton Therapy Center, Unit 130, The University of Texas M D Anderson Cancer Center, 1840 Old Spanish Trail, Houston, TX 77030, USA

E-mail: swpeters@mdanderson.org

Abstract

The purpose of this study is to validate the accuracy of a Monte Carlo calculation model of a proton magnetic beam scanning delivery nozzle developed using the Geant4 toolkit. The Monte Carlo model was used to produce depth dose and lateral profiles, which were compared to data measured in the clinical scanning treatment nozzle at several energies. Comparisons were also made between measured and simulated off-axis profiles to test the accuracy of the model's magnetic steering. Comparison of the 80% distal dose fall-off values for the measured and simulated depth dose profiles agreed to within 1 mm for the beam energies evaluated. Agreement of the full width at half maximum values for the measured and simulated lateral fluence profiles was within 1.3 mm for all energies. The position of measured and simulated spot positions for the magnetically steered beams agreed to within 0.7 mm of each other. Based on these results, we found that the Geant4 Monte Carlo model of the beam scanning nozzle has the ability to accurately predict depth dose profiles, lateral profiles perpendicular to the beam axis and magnetic steering of a proton beam during beam scanning proton therapy.

1. Introduction

The increased interest in proton therapy has lead to an increase in proton therapy centers worldwide and to ever increasing clinical demand. This demand has restricted the amount of proton beam time used for research purposes, and as a result has led to the increased use

[3] Author to whom any correspondence should be addressed.

of Monte Carlo based modeling as a substitute for beam measurements in proton research. Monte Carlo simulations have been used in areas such as, shielding calculations for proton therapy centers (Fan *et al* 2007, Newhauser *et al* 2002), calculations of secondary neutron doses (Polf and Newhauser 2005, Schneider *et al* 2002, Zheng *et al* 2007, Yan *et al* 2002), design and development of the passive scattering delivery technique and verification of proton treatment doses (Parodi *et al* 2007) and commissioning of clinical treatment planning systems (Newhauser *et al* 2007). Also, there has been a large amount of work specifically involving the validation of Monte Carlo calculated dose profiles for passive scattering proton treatment nozzles against measured data (Paganetti *et al* 2004, Polf *et al* 2007) and for patient-specific calibration and monitor unit calculations (Herault *et al* 2007).

Along with these applications, since the development of proton treatment delivery methods, such as magnetic spot scanning (Kanai *et al* 1983) and intensity modulated proton therapy (IMPT) (Lomax *et al* 1999), there has been a need for Monte Carlo to accurately simulate not only scattering and dose deposition processes, but the magnetic steering of protons as well. The use of Monte Carlo simulations to model proton treatment delivery with magnetic spot scanning has so far been rather limited; we believe in part due to the limited number of facilities worldwide (to date) using the beam scanning delivery technique. Tourovsky *et al* (2005) reported on the development of the Monte Carlo model used at the Paul Scherer Institute to calculate treatment doses that did not model magnetic steering of the proton beams, but instead simulated each pencil beam with a given energy spectrum, angular divergence and direction starting from the exit of the nozzle. Paganetti (2004) reported on the ability of the Geant4 Monte Carlo toolkit to model transport of the proton beam through the treatment nozzle, which included magnetic steering of the proton pencil beams during proton treatment delivery, and subsequently used a model of a proton scanning beam model to study the effects of tumor and organ motion on beam scanning treatment delivery (Paganetti *et al* 2005).

However, to our knowledge, the ability of the Geant4 Toolkit to accurately model proton beam scanning delivery, including magnetic steering, has not been reported in the literature. The purpose of this study is to determine the accuracy of a Geant4 Monte Carlo model of the proton magnetic beam scanning delivery technique. In particular, we were interested in the ability of Geant4 to accurately model magnetic beam steering using a simplified uniform magnetic field. To do this, we modeled all components in the University of Texas M. D. Anderson Proton Therapy Center-Houston (PTC-H) magnetic beam scanning nozzle that interact with the beam. For beam steering, we defined a uniform magnetic field within the steering magnets in the nozzle. Validation of our model included comparison of depth dose profiles in water, and in-air crossfield fluence profiles of both unsteered and magnetically steered beams to measured data for several different beam energies. Accuracy of the model was determined by comparing the distal 80% range, 90–10% distal dose falloff and 50–50% peak width for the calculated and measured depth dose profiles, and by comparing the beam axis position, full width half maximum (FWHM) and 10–10% width values of the calculated and measured lateral fluence profiles.

The computational simulations for the scanned beam proton therapy nozzle were performed using Geant4 (version 9.1, release date: 14 December 2007), a Monte Carlo toolkit composed of C++ libraries. Geant4 is an object-oriented environment with great flexibility and unrestricted control over the code. It was originally developed at CERN for high-energy applications, but is being applied in low-energy realms, particularly in medical physics. This development is on-going through a world-wide collaboration of scientists and software engineers. Some examples of use of Geant4 in the area of medical physics are validation of photon and electron simulations against other MC codes and against experimental
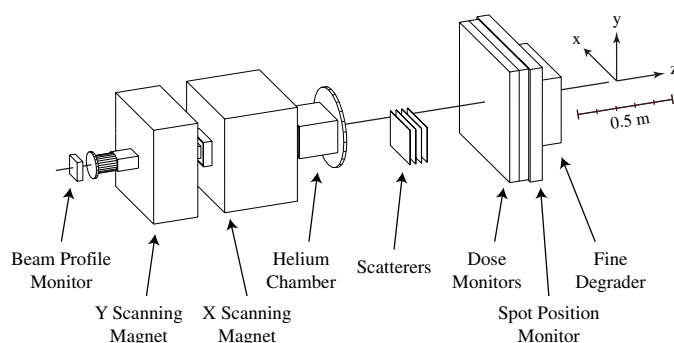
Figure 1. Schematic drawing of the PTC-H scanning beam nozzle with all components drawn to scale and labeled, including the two beam steering magnets and beam direction (*z*-direction). The nozzle is shown as modeled within the Geant4 Monte Carlo model with the exception of the scatterer and fine degrader, which were not yet clinically commissioned and thus not included in the model.

measurements from clinical linacs (Carrier *et al* 2004, Poon and Verhaegen 2005), and the Geant4 application for tomographic emission (GATE), creating realistic simulations for nuclear medicine imaging systems, PET and SPECT (De Beenhouwer *et al* 2007). Examples of Geant4 applications common to proton therapy include simulations of dose delivery with a passive scattering treatment nozzle (Paganetti *et al* 2004) and studies of the production of positron emitting isotopes during proton treatment (Parodi *et al* 2007).

2. Materials and methods

2.1. Monte Carlo model of the proton scanning beam nozzle

The Geant4 model of the PTC-H scanned beam proton treatment nozzle includes all components that directly interact with the beam as it is transported through the nozzle as shown in figure 1. Specifications for each modeled component were taken from the nozzle design documents provided by the manufacturer (Hitachi Corp.). The components included in the model start at the entrance of the nozzle with the titanium window on the end of the beam transport line, followed by an ionization chamber, consisting of two copper-coated polyimide windows and two sets of perpendicular tungsten wire meshes serving as the high-voltage electrodes, used to monitor the profile of the incident proton beam. Next, the beam travels through the first steering magnet, which can steer the beam in the *y*-direction, and is immediately followed by the second magnet, which controls beam steering in the *x*-direction. Traveling through the center of the steering magnets is a low-pressure stainless steel and ceramic helium gas chamber designed to reduce the amount of beam scatter in the nozzle. At each end of the helium chamber is a copper-coated polyimide window. After the helium chamber is a scattering device consisting of four plates of different material that can be moved in and out of the beam to enlarge the beam size if desired. The scatterer is followed by two parallel plate ionization chambers to measure the spot dose. The two dose monitors are identical and consist of three copper-coated polyimide electrodes with two copper-coated polyimide windows. The proton beam then passes through the spot position monitor, which has the same basic design as the beam profile monitor with a larger surface area in order to measure the position of all possible scanned proton beams passing through the nozzle. The last element in the nozzle is the fine degrader, used for fine control over the proton range. It

is composed of ten sheets of low-Z plastic with varying thickness that can be inserted and removed from the beam as needed. The simulation included a water phantom positioned with its front face at isocenter for dose calculations. The water phantom was removed for in-air fluence calculations. The fine degrader and scatterer nozzle elements are not currently commissioned for clinical use and are therefore not included in simulations carried out in this study. The proton range loss resulting from all elements in the scanning beam nozzle ranges from 0.3 to 0.5 g cm^{-2} for the beam energies used during treatment.

The two steering magnets in the scanned beam proton therapy nozzle independently control the deflection of the proton beam in the x- and y-directions perpendicular to the initial beam direction (along the z-axis in our model). The y-direction steering magnet is positioned so that the beam passes through it first, followed by the x-direction magnet. The length of each steering magnet was modeled according to the 'effective pole length' defined by the manufacturer. The effective pole length is found by integrating the magnetic field along the central beam axis and dividing by the maximum magnetic field value to estimate the length of a uniform magnetic field at the maximum value. The magnetic fields of the steering magnets were modeled as a uniform magnetic field filling the entire magnet volume and zero everywhere outside of the magnets. The transport of protons through the magnetic fields was solved in Geant4 using a fourth-order Runge–Kutta integration. The curved path of the proton is broken into sections, which were defined to be no greater than 0.01 mm. Each section is approximated by its chord in order to test for boundaries, intersections and particle collisions (Agostinelli *et al* 2003).

The Geant4 toolkit includes a comprehensive set of physics processes to handle electromagnetic and hadronic interactions, offering alternate models for most interactions. Three basic classes of models are implemented in Geant4, data-driven models, parameterization-driven models and theory-driven models. Data-driven models are considered the optimal modeling option, but can only be used where experimental data are available. The other two models fill in where there are gaps in the existing data. Each physics process is loaded individually into the 'physics list' where it is linked with the related particles, and the appropriate energy limits are set. The physics list is then used during simulation to determine when specific interactions occur.

Two basic packages are available in Geant4 to handle the electromagnetic interactions of leptons, photons, hadrons and ions: the standard model and the low-energy model. Both packages include the processes of ionization, bremsstrahlung, multiple scattering, Compton scattering, photoelectric effect, pair production and annihilation. The standard package extends from 10 keV up to 100 TeV and relies mostly on parameterizations of the cross-section data. The low-energy electromagnetic package extends the energy range down to 250 eV and includes Rayleigh scattering. Due to the importance of the atomic shell structure in the low-energy range, the photon and electron physics models make direct use of the shell cross-section data extracted from publicly distributed evaluated data libraries: EPDL97, EEDL and EADL. The low-energy process that handles hadron and atom ionization (G4hLowEnergyIonisation) depends on the Bethe–Bloch formula in the high-energy range (>2 MeV), the free electron model in the low-energy range (<1 MeV) and parameterized models based on experimental data in the intermediate range (between 1 MeV and 2 MeV). This intermediate energy interval is important in the physics list for calculation of proton treatment doses since it represents the range of proton energies encountered at the end of proton range near the distal edge of the Bragg peak.

The multiple scattering model in Geant4 (G4MultipleScattering) was developed by Urbán (2002) and is based on the theory introduced by Lewis (1950). This model, used for all charged particles, is a condensed simulation algorithm, which simulates the scattering of a particle by

computing the path length correction and the lateral displacement. Modeling of fluctuations in the continuous energy loss, or 'energy straggling,' of charged particles in Geant4 is taken into account using two different straggling models. For regions with a low number of delta-rays produced, energy loss fluctuations are modeled by the faster Gaussian distribution with Bohr's variance. This model is used when the continuous energy loss over a track segment is ten times greater than the electron kinetic energy cut. In regions where there is significant delta-ray production, the fluctuations are modeled by a two-energy-level model of the atom (Wellisch *et al* 2007).

Geant4 provides an extensive list of models governing the hadronic interactions. In this study, we modeled the proton–nuclear interactions with low-energy processes for elastic and inelastic scattering. The default elastic scattering process (G4LElastic), which handles the elastic scattering of all hadrons, was used. For the inelastic scattering process, several models exist and none cover all hadrons, so based on results of several previous studies (Aso *et al* 2005, Cirrone *et al* 2005, Paganetti *et al* 2004), we used the theory-driven 'precompound' model and the default parameterization-based 'low-energy inelastic' model. However, unlike these previous studies, we did not incorporate an energy cutoff for the two nuclear models; instead better agreement was achieved when the 'precompound' model (G4PreCompoundModel) was used for inelastic scattering for all hadrons, including protons, neutrons and pions at all energies and the 'low-energy inelastic' model was used for all ions. For the low-energy hadron ionization physics process, the parameterization for the intermediate energy based on ICRU–49 (1993) gave us better agreement with measured data than the alternate models based on work done by Ziegler (Anderson and Ziegler 1977, Ziegler *et al* 1985).

Control of particle transportation during simulation plays an important part in the accuracy with which the physics processes are modeled. Two particular control parameters were applied to the particle transport during simulation, maximum step size and range cuts. Maximum step size sets an upper limit on the distance a particle travels before its status is re-evaluated. Range cuts are used to determine the lower-energy limit at which a particle should no longer be tracked and its remaining energy deposited locally. Geant4 uses a range cutoff instead of an energy cutoff in order to have a more coherent definition across all materials and particles included within the simulation. It is also possible to set a lowest-energy limit in conjunction with the range cut, which determines the energy where all particles are no longer tracked. Geant4 is capable of defining range cuts and step size values that are specific to particular regions within the simulated geometry. For our simulations, a 1 mm particle step size was used throughout the geometry, except inside the water phantom where the maximum step size was set to 0.2 mm to ensure the step size was not larger than the tally resolution of 0.2 mm. The range cut inside the water phantom was set to 0.01 mm while the default value (1 mm) was used throughout the remaining geometry. The lowest-energy limit for tracking particles was set to 1 keV for all particles throughout the simulated geometry.

The PTC-H proton beam as it enters the scanning beam nozzle was characterized by the manufacturer (Hitachi Corp.) during initial acceptance testing of the nozzle. For our model, the initial energy distribution of the proton beam was defined with a Gaussian distribution with sigma values provided by Hitachi. The initial position and angular distributions of the protons were based on the emittance values also specified by the manufacturer. The scanning nozzle is also configured for use with a focused proton beam with the focal point being the isocenter. That is, the beam is focused such that if it were propagated in a vacuum without nozzle elements, it would converge to a point at isocenter. The Monte Carlo model duplicates this focusing of the particle beam by setting the initial angular trajectory of each proton toward the isocenter. The beam focusing and initial divergence were combined with the initial beam profiles to reproduce the overall beam emittance values of 4.2–8.4 mm

mrad along the *x*-direction and 0.3–0.6 mm mrad along the *y*-direction as specified by the manufacturer.

2.2. Validation measurement and simulations

Calculations made with our model of central axis depth dose in water and in-air crossfield fluence profiles were validated against measured data. The depth dose profiles were measured in a water tank (Scanditronix Blue Phantom), positioned with the front face at the isocenter. The measurements were made as a part of the clinical commissioning with an 8 cm diameter ion chamber (PTW T34070) at the three initial beam energies (72.5, 139.8, 219.3 MeV) used in this study. The depth dose profiles were calculated during simulation in a ROOT histogram (Brun and Rademakers 1997), recording the energy deposited by every interaction occurring within the tally volume. The lateral dimensions of the depth dose histogram reproduced the dimensions of the 8 cm diameter ion chamber used during measurements. The resolution along the beam central axis was set to 0.2 mm for the low- and medium-energy (72.5 and 139.8 MeV) beams and 0.8 mm for the high-energy (219.3 MeV) beam to match the spacing of the measurements.

The lateral profiles of the proton beam were measured in air using self-developing Gafchromic EBT film (International Specialty Products, Wayne, NJ) placed perpendicular to the beam central axis. The initial beam energies used for measurements of the lateral profiles were 72.5, 139.8 and 219.3 MeV. The lateral profile measurements were performed with two different spot configurations. The first configuration consisted of a central on-axis pencil beam surrounded by four magnetically steered proton pencil beams extending from -5 to $+5$ cm along the *x*-axis and from -6 to $+6$ cm along the *y*-axis. The second configuration consisted of a series of off-axis spots at the following (*x*, *y*) positions: (3, 3), (3, 15), (13, 3) and (13, 15). For each initial energy and each configuration, three measurements were made along the beam central axis (*z*-direction), 15 cm upstream from isocenter ($z = -15$ cm), at isocenter ($z = 0$ cm) and 15 cm downstream ($z = 15$ cm) from isocenter. The EBT film was scanned on a commercial Epson 10000 XL flatbed scanner (Epson America, Long Beach, CA) and the calibration curve used to convert the data from optical density to dose was a cubic polynomial obtained from an X2-fit with the data points. More details about the procedure used to analyze the EBT film is described in Ciangaru *et al* (2007).

Calculations of the lateral fluence profiles were performed in air at the three initial energies listed above. The lateral profiles were stored in a ROOT histogram set to tally proton fluence in a two-dimensional grid in the plane perpendicular to the beam central axis (*z*-axis from figure 1). The grid voxel size was 0.35 mm^2 for the lateral profiles, mimicking the spatial resolution used for scanning of the EBT film. The calculation at each energy and spot configuration simulated the on and off-axis lateral profiles at the three measurement positions along the beam axis. Using the magnetic field values used during the measurements, calculations of all profiles were performed within a single simulation, taking advantage of Geant4's ability to change the magnetic field values during simulation. All simulations were run on a 1024-cpu institutional cluster with the length of the simulation depending on the initial beam energy and the profile type. For the depth dose profiles, ten million protons required about 100, 180 and 300 h on a single cpu for the 72.5, 139.8 and 219.3 MeV beam energies, respectively. For the lateral profiles, ten million protons required about 185, 175 and 170 h on a single cpu for the 72.5, 139.8 and 219.3 MeV beam energies, respectively. The addition of the magnetic field to the Monte Carlo model to steer the off-axis spots resulted in a 3–4% increase in calculation time over unsteered on-axis spots.

Overall uncertainty in the spot position and beam profiles resulted from uncertainties in both the Monte Carlo calculations and the measurements. To ensure statistical accuracy
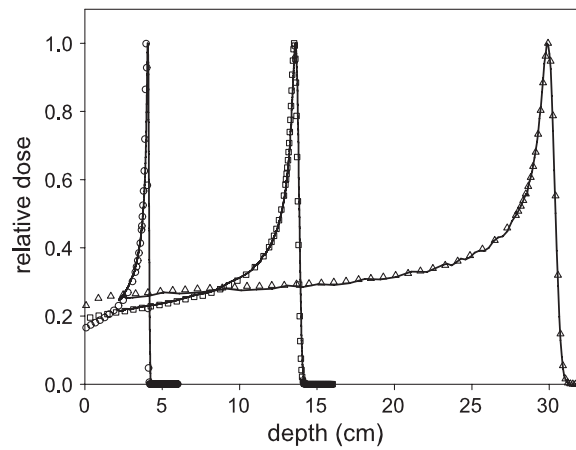
Figure 2. Measured (line) and simulated (symbols) depth dose profiles along the z-axis within a water phantom for beam energies of 72.5 (left), 139.8 (middle) and 219.3 MeV (right). Data are normalized to the maximum dose values. Uncertainties in measurements and calculations are smaller than symbols. For display purposes, not all simulated data points are shown.
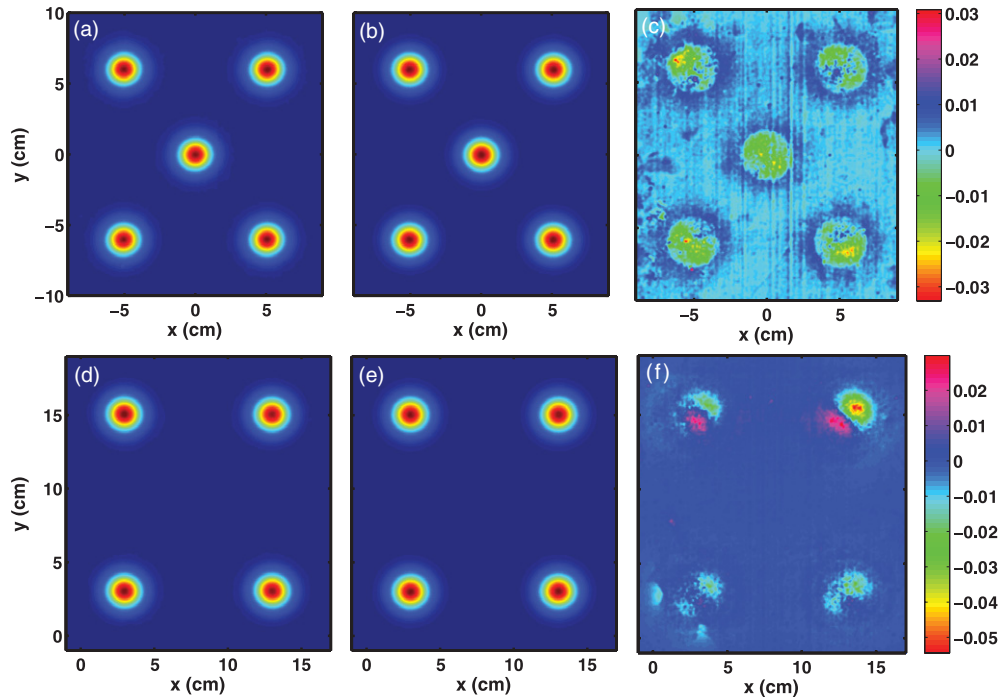
Figure 3. Lateral in-air fluence profiles of the measured (a), (d) and simulated (b), (e) 139.8 MeV spots perpendicular to the beam direction (z-axis) at isocenter. The difference (c), (f) between the data was found by normalizing each set of data and subtracting the simulated data from the measured data. The profiles are normalized to the measured peak value at (0, 0) for panes (a)–(c) and to the measured peak at (3, 3) for panes (d)–(f).

(This figure is in colour only in the electronic version)
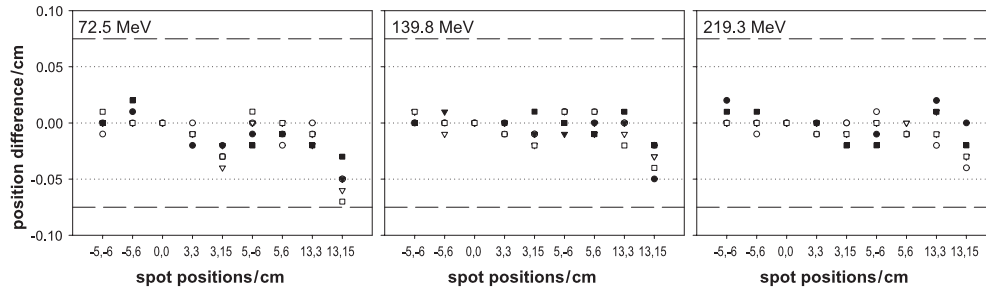
Figure 4. Difference between the measured and calculated positions for the each of the nine lateral profiles along the *x* (solid symbols) and *y* (empty symbols) directions at $z = -15$ cm (circles), 0 cm (triangles) and 15 cm (squares) positions along the beam direction. The position differences are within the maximum expected uncertainty value of 0.75 mm (dashed line) for all energies and *z*-positions.
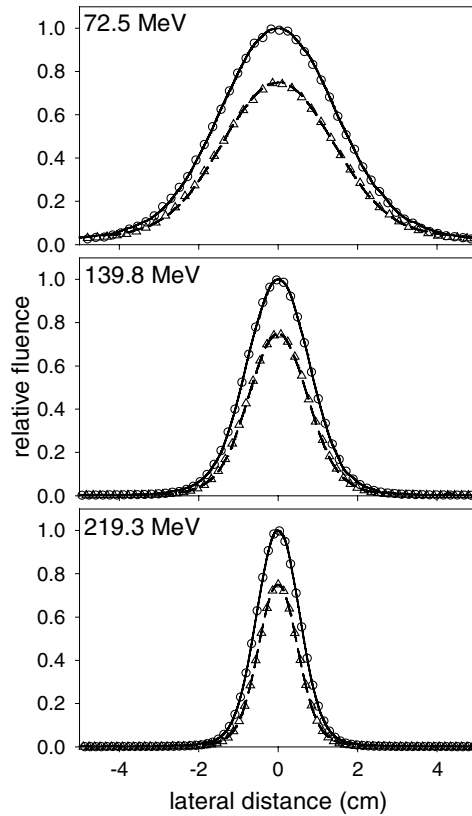
Figure 5. Measured (lines) and simulated (symbols) lateral in-air on-axis fluence profiles along the *x*- and *y*-axes at isocenter for the 72.5, 139.8 and 219.3 MeV beam energies. The simulated data are normalized to the central axis measured data values. The *y*-axis measured (dashed line) and simulated (triangles) profiles are multiplied by 0.75 for display purposes. Uncertainties in measurements and calculations are smaller than symbols. For display purposes, not all data points are shown.
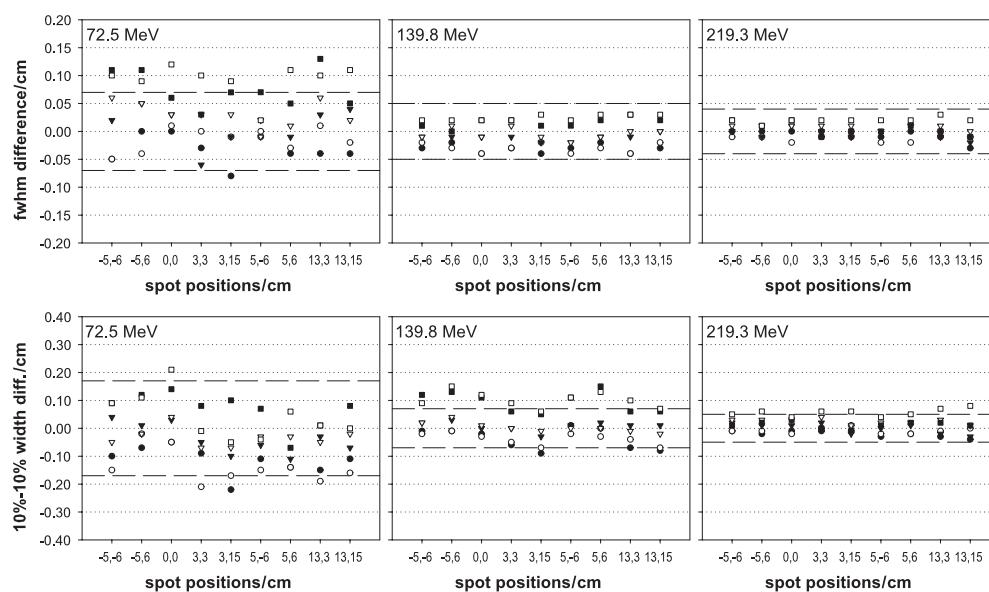
Figure 6. Comparison of the nine measured and calculated lateral profiles along the x (solid symbols) and y (empty symbols) directions at $z = -15$ cm (circles), 0 cm (triangles) and 15 cm (squares) positions along the beam direction. The FWHM and 10–10% widths agree to within 1.3 and 2.2 mm, respectively, for all energies and z-positions. The dashed lines represent the maximum estimated uncertainty at each energy.

of the simulated results, each depth dose profile simulation was calculated using ten million proton histories in order to produce a 1-sigma relative statistical uncertainty of less than 1% throughout the distribution. For the lateral fluence profiles, due to the smaller voxel sizes used for the calculations, 100 million histories per spot position were required to obtain a similar level of statistical uncertainty (less than 1%) near the peak and up to 3% at the 10% dose level. The lateral profile fluence uncertainties translated into position uncertainties in the calculated profiles at the 10% dose level of 0.6 mm, 0.25 mm and 0.1 mm for the low, medium and high energies, respectively. For the measurements, uncertainties in the measured values were due to both the resolution of the EBT films and film scanner, and due to uncertainty in the proton beam delivery caused by fluctuations in the initial proton beam alignment and fluctuations in the magnetic field strength within the steering magnets. The inherent resolution of the film itself is very high (the intermolecular distances), but the final data resolution is limited by the scanning resolution, which was 72 dpi (0.35 mm pixel^{-1}) in this case. The dose uncertainty in the EBT film is estimated to be about 1% at the profile peak and 5% at the 10% dose level, which translated into position uncertainties in the measured profiles at the 10% dose level of 1.4 mm, 0.55 mm and 0.3 mm for the low, medium and high energies, respectively. Beam delivery fluctuations result in a position-dependent spot position uncertainty, as estimated by the manufacturer, ranging from less than 0.6 mm for on-axis (unsteered) beams up to 0.75 mm for the maximum beam steering considered in this work ($x = 13$ cm, $y = 15$ cm).

3. Results and discussion

Measured and calculated depth dose profiles for initial beam energies of 72.5, 139.8 and 219.3 MeV are shown in figure 2 with the profiles normalized to the maximum values. The depth of the measured and calculated 80% distal dose fall-off values for all three beam energies
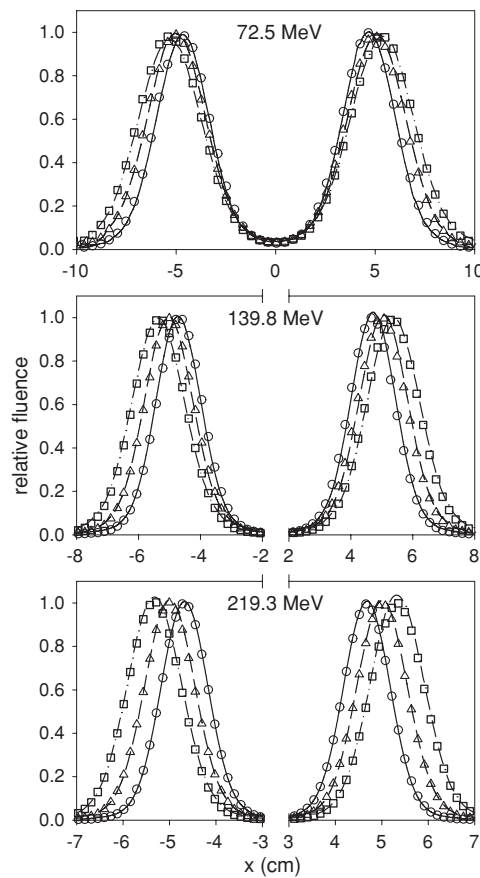
Figure 7. Cross sections of the measured (line) and the simulated (symbols) off-axis lateral profiles at the three *z*-positions: 15 cm upstream (solid line, circles), at isocenter (dashed line, triangles), 15 cm downstream (dot-dashed line, squares). The cross sections were taken at the center of each spot profile for the upstream, isocenter and downstream positions, corresponding to *y* = 5.68, 6.00 and 6.33 cm, respectively. Uncertainties in measurements and calculations are smaller than symbols. For display purposes, not all data points are shown.

was found to agree to 1 mm or better. The comparison of measured and simulated 90–10% distal fall-off and 50–50% width values for all three energies was found to agree within 0.01 mm and 0.8 mm, respectively.

The measured and simulated fluence profiles for the 139.8 MeV incident energy is shown in figure 3. The pattern of the two spot configurations can be seen in figure 3, as well as the difference between the measured and simulated results at isocenter for the 139.8 MeV beam energy. Figure 4 shows the difference between the final position of the measured and simulated spots. The final 'spot positions' were defined as the *x*-coordinate and *y*-coordinate of the peak of the measured beam spot. The positions of the measured and simulated off-axis spots agreed within the expected uncertainty, with the final peak position of all calculated spots being within 0.7 mm of the measured position.

Figure 5 shows the lateral profiles measured on the beam central axis (center spot in figure 3(a)) at isocenter for 72.5, 139.8 and 219.3 MeV beam energies with their corresponding normalized Monte Carlo simulation results. The lateral profiles were compared by measuring the full width at half maximum and the distance from 10% dose level to 10% dose level

(10–10% width) of each spot profile along the *x*- and *y*-axes at the three different beam axis (*z*-axis) positions. Figure 6 shows the difference between the measured FWHM and 10–10% widths at each of three beam energies, including the expected maximum uncertainty for each set of data. For the 72.5 MeV beam, all the FWHM values agreed within 1.3 mm, with 42 of the 54 spots agreeing within the uncertainty value of 0.7 mm, while the 10–10% widths all agreed within 2.2 mm, with 50 of the 54 spots agreeing within the uncertainty value of 1.7 mm. For the 139.8 MeV beams, the largest difference between measured and simulated data for the FWHM was 0.4 mm, which was within the uncertainty value of 0.5 mm, while the largest 10–10% width difference was 1.5 mm, with 40 of the 54 spots agreeing within the estimated uncertainty value of 0.7 mm. The FWHM values for the highest-energy beam all agreed within the uncertainty value of 0.4 mm and the largest 10–10% width difference was 0.8 mm, with 49 of the 54 spots agreeing within the uncertainty value of 0.5 mm.

Figure 7 shows the *x*-direction cross-sectional comparison of the measured and simulated off-axis profiles at the three different *z*-positions. The three cross sections are taken along the *x*-direction at the *y*-position corresponding to the calculated peak value for the spot. The off-axis profiles in figure 7 demonstrate the shift of the spots away from isocenter as the *z*-position increases, as well as, the linear increase of beam width with *z*-position, both traits of a diverging particle beam subjected to Coulomb scattering. Although the lateral profile calculations modeled the measured profiles within or close to the expected uncertainty values, we noticed that the shape of the measured and calculated spot profiles varied significantly from that of a Gaussian, particularly near the 'tail' of the spot profile. In fact, it has been shown that the overall shape of the spot profiles can be better described by the convolution of three Gaussians for both the measured and calculated lateral profiles (Ciangaru *et al* 2005, Lax *et al* 1983).

4. Conclusion

We have developed a Geant4 Monte Carlo model of the beam scanning nozzle at the M.D. Anderson Proton Therapy Center-Houston, with the ability to reproduce measured data and model the magnetic beam steering. The depth of the distal 80% dose, distal 90–10% dose falloff and 50–50% width of the simulated depth dose profiles all agreed with the experimental data to within 1 mm. For the lateral fluence profiles, agreement was within the uncertainty of the measured and simulated FWHM values at the medium and high energies, while at the low energy, 43 of the 54 FWHM difference values were within the uncertainty. The lateral profile 10–10% widths showed differences up to 2.2 mm at the lowest energy, with 139 of the 162 spots across the three energies agreeing within their respective uncertainty values.

The Geant4 magnetic interaction models were used to simulate lateral steering of the proton beams. All final spot positions of the lateral profiles of the steered beams calculated with the Monte Carlo model agreed with the measured position of steered beams upstream from, downstream from and at isocenter to within 0.7 mm. For our simulations, we modeled the steering magnets as uniform magnetic fields with magnetic pole lengths set according to the manufacturer-provided effective magnetic pole length values. This simple model provided a good approximation of the actual beam steering process and produced agreement between measured and simulated spot positions to within the expected uncertainty of the beam delivery system. However, figure 4 shows that the difference between measured and simulated position did increase with increasing *x*- and *y*-positions, up to 0.7 mm at the $x = 13$, $y = 15$ cm spot in the 15 cm downstream lateral profile. This result is not all together unexpected, since the uncertainty in the final position of the beam spot increases as the magnetic field strength used for beam steering increases. We believe that if better agreement is required, that it could

possibly be achieved through the use of a more sophisticated model of the magnetic field shape within the steering magnet.

Comparisons of the measured and simulated beam shape (FWHM) produced agreement within uncertainty at the medium and high beam energies. However, some of the low-energy profile differences between measured and calculated FWHM values were outside the expected values (almost all profiles at the downstream position ($z = 15$ cm)). This trend continues for the beam shape at the 10% dose level, with 17 of the 23 width values outside the expected uncertainty occurring at the downstream position. The data suggest a systematic shift in beam width, with the simulated lateral profile beam widths being slightly larger than measured beam widths upstream and slightly smaller than measured beam widths downstream. Another factor, particularly with the 10–10% dose width differences, may be inaccuracies in the EBT film at low doses. The measurements made with the EBT film must be irradiated with a large enough dose to get sufficient dose reading above the background values. At the 10% dose level, the lower dose is hard to separate from the background resulting in greater noise, possibly greater than the 5% estimated dose uncertainty. We also believe the level of agreement could be improved through small adjustments to the beam emittance values. Although all data shown in this paper used the measured emittance values provided by the manufacturer, we believe these adjustments could be justified, since the provided beam emittance values were from preliminary measurements made prior to final beam commissioning and may not reflect the exact values at the time of our measurements.

From this, we conclude that a sophisticated model of the magnetic field used for beam steering may not necessarily be needed to accurately model the beam steering process. Based on our comparison between the measured and simulated profiles, we have shown that by using a uniform magnetic field model for beam steering, Geant4 can predict the final spot position and changes in the width of the beam profile with a sufficient degree of accuracy (within measurement uncertainties). Even for the discrepancies seen in downstream beam profiles for the lowest- and medium-energy beams, the largest differences also occurred for the unsteered, on-axis beams, leading us to believe that the discrepancies may not be due to the simple magnetic field model. Since the largest differences were seen for the low- and medium-energy profiles, this leads us to believe that the differences seen for the lower energies may instead lie in part with the accuracy of the scattering models used with the Geant4 toolkit at lower proton energies. The discrepancies in beam shape at the 10% dose level and below are the subject of several on-going investigations at the U T M. D. Anderson Proton Therapy Center.

Based on this level of agreement between measurements and calculations we conclude the Geant4 beam model described in this paper can be used to accurately predict the depth dose profiles, and changes to the lateral fluence profiles due to magnetic steering for scanned beam proton therapy for medium- and high-energy beams. However, based on the level of disagreement in the measurements and calculations in the tail region of the beam profiles for the 72.5 MeV beam, we would recommend that precautions be taken to account for these differences in calculations made for the lower proton energies. As part of on-going work to evaluate the beam scanning treatment nozzle, the Geant4 Monte Carlo model will be used in future studies of magnetic beam scanning, such as variations in magnetic steering, scanned beam nozzle design studies, quality assurance studies and treatment planning verification.

References

Agostinelli S *et al* 2003 GEANT4-a simulation toolkit *Nucl. Instrum. Methods Phys. Res.* A **506** 250–303
Anderson H H and Ziegler J F 1977 *The Stopping and Range of Ions in Matter* vol 3 (New York: Pergamon)
Aso T, Kimura A, Tanaka S, Yoshida H, Kanematsu N, Sasaki T and Akagi T 2005 Verification of the dose distributions with GEANT4 simulation for proton therapy *IEEE Trans. Nucl. Sci.* **52** 896–901

Brun R and Rademakers F 1997 ROOT—an object oriented data analysis framework *Nucl. Instrum. Methods Phys. Res.* A **389** 81–6

Carrier J F, Archambault L, Beaulieu L and Roy R 2004 Validation of GEANT4, an object-oriented Monte Carlo toolkit, for simulations in medical physics *Med. Phys.* **31** 484–92

Ciangaru G *et al* 2007 Verification procedure for isocentric alignment of proton beams *J. Appl. Clin. Med. Phys.* **8** 2671

Ciangaru G, Polf J C, Bues M and Smith A R 2005 Benchmarking analytical calculations of proton doses in heterogeneous matter *Med. Phys.* **32** 3511–23

Cirrone G A P, Cuttone G, Guatelli S, Lo Nigro S, Mascialino B, Pia M G, Raffaele L, Russo G and Sabini M G 2005 Implementation of a new Monte Carlo–GEANT4 simulation tool for the development of a proton therapy beam line and verification of the related dose distributions *IEEE Trans. Nucl. Sci.* **52** 262–5

De Beenhouwer J, Staelens S, Kruecker D, Ferrer L, D'Asseler Y, Lemahieu I and Rannou F R 2007 Cluster computing software for GATE simulations *Med. Phys.* **34** 1926–33

Fan J, Luo W, Fourkal E, Lin T, Li J, Veltchev I and Ma C M 2007 Shielding design for a laser-accelerated proton therapy system *Phys. Med. Biol.* **52** 3913–30

Herault J, Iborra N, Serrano B and Chauvel P 2007 Spread-out Bragg peak and monitor units calculation with the Monte Carlo code MCNPX *Med. Phys.* **34** 680–8

ICRU 1993 *Stopping Powers and Ranges for Protons and Alpha Particles* (Bethesda, MD: International Commission on Radiation Units and Measurements)

Kanai T, Kawachi K, Matsuzawa H and Inada T 1983 3-dimensional beam scanning for proton therapy *Nucl. Instrum. Methods Phys. Res.* **214** 491–6

Lax I, Brahme A and Andreo P 1983 Electron beam dose planning using Gaussian beams. Improved radial dose profiles *Acta Radiol. Suppl.* **364** 49–59

Lewis H W 1950 Multiple scattering in an infinite medium *Phys. Rev.* **78** 526

Lomax A J, Bortfeld T, Goitein G, Debus J, Dykstra C, Tercier P A, Coucke P A and Mirimanoff R O 1999 A treatment planning inter-comparison of proton and intensity modulated photon radiotherapy *Radiother. Oncol.* **51** 257–71

Newhauser W, Fontenot J, Zheng Y, Polf J, Titt U, Koch N, Zhang X and Mohan R 2007 Monte Carlo simulations for configuring and testing an analytical proton dose-calculation algorithm *Phys. Med. Biol.* **52** 4569–84

Newhauser W D, Titt U, Dexheimer D, Yan X and Nill S 2002 Neutron shielding verification measurements and simulations for a 235-MeV proton therapy center *Nucl. Instrum. Methods Phys. Res.* A **476** 80–4

Paganetti H 2004 Four-dimensional Monte Carlo simulation of time-dependent geometries *Phys. Med. Biol.* **49** N75–81

Paganetti H, Jiang H, Lee S Y and Kooy H M 2004 Accurate Monte Carlo simulations for nozzle design, commissioning and quality assurance for a proton radiation therapy facility *Med. Phys.* **31** 2107–18

Paganetti H, Jiang H and Trofimov A 2005 4D Monte Carlo simulation of proton beam scanning: modelling of variations in time and space to study the interplay between scanning pattern and time-dependent patient geometry *Phys. Med. Biol.* **50** 983–90

Parodi K, Paganetti H, Cascio E, Flanz J B, Bonab A A, Alpert N M, Lohmann K and Bortfeld T 2007 PET/CT imaging for treatment verification after proton therapy: a study with plastic phantoms and metallic implants *Med. Phys.* **34** 419–35

Polf J C, Harvey M C, Titt U, Newhauser W D and Smith A R 2007 Initial beam size study for passive scatter proton therapy. I. Monte Carlo verification *Med. Phys.* **34** 4213–8

Polf J C and Newhauser W D 2005 Calculations of neutron dose equivalent exposures from range-modulated proton therapy beams *Phys. Med. Biol.* **50** 3859–73

Poon E and Verhaegen F 2005 Accuracy of the photon and electron physics in GEANT4 for radiotherapy applications *Med. Phys.* **32** 1696–711

Schneider U, Agosteo S, Pedroni E and Besserer J 2002 Secondary neutron dose during proton therapy using spot scanning *Int. J. Radiat. Oncol. Biol. Phys.* **53** 244–51

Tourovsky A, Lomax A J, Schneider U and Pedroni E 2005 Monte Carlo dose calculations for spot scanned proton therapy *Phys. Med. Biol.* **50** 971–81

Urbán L 2002 Multiple scattering model in Geant4 CERN-OPEN-2002–070

Wellisch H, Maire M and Urban L 2007 *Geant4 Physics Reference Manual* v9.1 http://www.geant4.org/geant4/support/userdocuments.shtml (accessed 14 December 2007)

Yan X, Titt U, Koehler A M and Newhauser W D 2002 Measurement of neutron dose equivalent to proton therapy patients outside of the proton radiation field *Nucl. Instrum. Methods Phys. Res.* A **476** 429–34

Zheng Y S, Newhauser W, Fontenot J, Koch N and Mohan R 2007 Monte Carlo simulations of stray neutron radiation exposures in proton therapy *J. Nucl. Mater.* **361** 289–97

Ziegler J F, Biersack J P and Littmark U 1985 *The Stopping and Range of Ions in Solids* vol 1 (New York: Pergamon)